INSTITUT DE FRANCE
Académie des sciences

Comptes Rendus

Chimie

Farida Bouyahmed, Fabrice Muller, Annie Richard, Toufik Amayas Mostefaoui, Imad Belabbas, Fabienne Warmont, Marjorie Roulet, Laurence Reinert, Laurent Duclaux and Sandrine Delpeux-Ouldriane

Chitosan-multilayered graphene oxide hybrid beads for Zn^{2+} and metoprolol adsorption

Volume 25 (2022), p. 205-223

Published online: 6 September 2022

https://doi.org/10.5802/crchim.183

This article is licensed under the
Creative Commons Attribution 4.0 International License.
http://creativecommons.org/licenses/by/4.0/

Les Comptes Rendus. Chimie *sont membres du*
Centre Mersenne pour l'édition scientifique ouverte
www.centre-mersenne.org
e-ISSN : 1878-1543

Comptes Rendus
Chimie
2022, Vol. 25, p. 205-223
https://doi.org/10.5802/crchim.183

Full paper / *Article*

Chitosan-multilayered graphene oxide hybrid beads for Zn^{2+} and metoprolol adsorption

Farida Bouyahmed [*, a, b], Fabrice Muller [a, c], Annie Richard [d], Toufik Amayas Mostefaoui [b, e], Imad Belabbas [b], Fabienne Warmont [a], Marjorie Roulet [a], Laurence Reinert [f], Laurent Duclaux [f] and Sandrine Delpeux-Ouldriane [a]

[a] CNRS-ICMN, Université d'Orléans, 45071 Orléans cedex 2, France

[b] Laboratoire de Physico-Chimie des Matériaux et Catalyse, Département de chimie, Faculté des Sciences Exactes, Université de Bejaia, Bejaia 06000, Algérie

[c] ISTO, Université d'Orléans, 45071 Orléans, France

[d] CME, Université d'Orléans, 45100 Orléans, France

[e] Thunder Optics, 34060, Montpellier, France

[f] Université Savoie Mont Blanc, EDYTEM, 73000 Chambéry, France

E-mails: f.bouyahmed@gmail.com (F. Bouyahmed), fabrice.muller@univ-orleans.fr (F. Muller), annie.richard@univ-orleans.fr (A. Richard), toufik.amayas@gmail.com (T. A. Mostefaoui), belabbas_imad@yahoo.fr (I. Belabbas), Fabienne.Warmont@cnrs-orleans.fr (F. Warmont), Marjorie.Roulet@univ-orleans.fr (M. Roulet), laurence.reinert@univ-savoie.fr (L. Reinert), laurent.duclaux@univ-smb.fr (L. Duclaux), sandrine.delpeux@cnrs-orleans.fr (S. Delpeux-Ouldriane)

Abstract. Chitosan (CS) hydrogel beads and hybrid beads made of a blending of CS hydrogels and Multilayer Graphene Oxide (MGO) were synthesized. The hybrid beads were prepared by gelation in NaOH solution of a 1 wt% CS acid solution with addition of MGO at either 1.5 wt% or 3 wt% loading rates. Prepared beads were characterized by infrared spectroscopy, thermogravimetric analysis (TGA), scanning electron cryo-microscopy and Brunauer–Emmett–Teller (BET) specific surface area measurements. Zn^{2+} and Metoprolol (MTP) adsorption kinetics and isotherms were studied on the pristine and hybrid CS hydrogel beads. The adsorption kinetics of Zn^{2+} and MTP in hybrid beads is limited by the diffusion to the MGO sites depending on their accessibility. While pure CS is not efficient for the MTP adsorption, the Langmuir-type isotherms of the 3 wt% MGO hydrogel beads (dose: 5 mg/100 mL) show 163 mg·g^{-1} maximum adsorption uptake. The MTP adsorption kinetics and isotherm suggest a MTP trapping on the MGO anionic sites (carboxylate groups) by electrostatic interactions. The Zn^{2+} adsorption capacities are the highest for the 3 wt% MGO hydrogel beads (236 mg·g^{-1}), and only of 40 mg·g^{-1} for the pure CS beads. The presence of Zn^{2+} adsorption sites in the hybrid bead, such as MGO carboxylate groups giving electrostatic interactions, and CS amine groups leading to complexation, provides synergic adsorption effects. The competitive adsorption of Zn^{2+} with respect to MTP in equimolar mixture was observed on hybrid beads (dose: 200 mg/100 mL) at 2 mmol·L^{-1} initial total

* Corresponding author.

concentration. At pollutant initial total concentration lower than 1.5 mmol·L^{-1}, no competition occurs. The regeneration at pH 4 of the hybrid beads toward MTP or Zn^{2+} adsorption was found to be 35–40% of the initial adsorption uptake for five adsorption/regeneration cycles.

Keywords. Chitosan, Multilayer graphene oxide, Water treatment, Zn^{2+}, Metoprolol.
Manuscript received 21 March 2021, revised 29 March 2022, accepted 20 April 2022.

1. Introduction

The non-biodegradable pollutant substances like metals and many organic molecules have significant environmental consequences and impact on human health. For example, Zn^{2+} and Metoprolol (MTP) are chemical pollutants frequently detected in waste water treatment plants (WWTP) and thus in surface water [1,2]. MTP is a beta blocker pharmaceutical highly prescribed against cardiovascular diseases. Its low biodegradability and the fact that almost 10% of the applied MTP dose is excreted unchanged, make it being present at the exhaust of WWTP at concentrations varying from 0.6 to 2.0 μg·L^{-1} [3,4].

Zinc most commonly enters the domestic water supply due to the deterioration of galvanized iron sheets and the dezincification of brass. The presence of zinc in water may also result from industrial waste pollution from steel work, mining, petrochemical industries, and agriculture. The World Health Organization standard, limiting the maximum contaminant level of hazardous substances, is 5 mg·L^{-1} for zinc in drinking water [5,6]. In France, its pollution limitation standard for surface water is 2 mg·L^{-1} if the pollutant flow is less than 10 g/day.

In order to purify water, many techniques have been developed such as co-precipitation [7,8], electrochemical method [9], ion exchange [10], coagulation, coagulation–flocculation, adsorption, reverse osmosis, photodegradation [11,12] and photocatalysis [11], etc. Adsorption is effective and one of the cheapest methods. In addition, the adsorbent regeneration can make this method cost-effective and sustainable [13–15].

Removal of MTP cation from water at neutral pH by adsorption was studied on different adsorbents. The magnetic carrageenan–silica hybrid nanoparticles show a high adsorption capacity of 447 mg·g^{-1} [16], whereas non-swelling clay minerals present lower uptakes: 7 mg·g^{-1} for kaolinite and 4 mg·g^{-1} for talc [17]. Metal ions such as Zn^{2+}, are known to be removed by various mineral adsorbents such as clay minerals [18], activated carbons (ACs) [19] and biopolymers [20–22] such as chitosan (CS). CS-based materials containing clay minerals and/or ACs were also used successfully for MTP removal by adsorption, as an adsorption capacity of 19 mg·g^{-1} was previously reported [23].

CS is a biodegradable, non-toxic polysaccharide prepared from the deacetylation of chitin which is after cellulose the most abundant biopolymer [24]. The use of CS for wastewater treatment has an ecological and economical interest due to its versatility and high adsorption capacity towards the di-cationic metals. Moreover, CS can be used in different forms: powder, beads [25], films [26] or sponges [27]. As CS contains hydroxyl and amine groups (Figure 1b) it can interact either with anionic or cationic pollutants depending on pH.

However, the CS use is limited by its dissolution in acidic medium at pH < 5 and by the accessibility of its adsorption sites [28] depending on its three-dimensional structure (Figure 1b). At a neutral pH value, CS adsorbs metal ions by complexation using the non-binding pairs of nitrogen and oxygen atoms, such as the complexation of Zn^{2+} [29,30] or Hg^{2+} ions [31]. In order to improve the physicochemical properties of CS and increase its resistance to acids, modifications such as carboxyalkylation [32] or crosslinking with glutaraldehyde [25] are necessary. However, these modifications involving the amine groups can significantly reduce the amount of available adsorption sites on CS [33].

In recent years, researchers have focused on the development of hybrid adsorbent of CS with carbon [34] or oxide particles to implement high adsorption capacity and synergic effects between the components. Jiang *et al.* [35] prepared beads of CS and Fe_3O_4 particles to apply the magnetic separation from water and increase the adsorption sites for Cu^{2+} removal. By mixing CS with multi-walled carbon nanotubes, Shawky *et al.* [15] obtained a composite with higher mechanical properties than CS providing additional adsorption sites. By mixing CS and ACs, high porosity hybrid beads were prepared with Cd^{2+} adsorption capacity (52.63 mg·g^{-1}) five times that of

pure CS [13]. In addition, the AC presence in CS creates hydrophobic sites, enabling the trapping of aromatic pollutants and widening the adsorption spectrum [23].

The Graphite Oxide (GO) or Multilayered Graphene Oxide (MGO) incorporation in CS makes it possible to obtain a hybrid material combining the CS and MGO adsorption properties [36]. Indeed, due to its negatively charged functional groups [37] (mainly, carboxyl and epoxy on the surface and edges of the planes), MGO (Figure 1a) is an efficient adsorbent for cationic pollutants such as Zn^{2+} [6], Cu^{2+} [38] and cationic dyes [39–43]. The maximum adsorption capacity of MGO for Zn^{2+} was found to be up to 246 $mg{\cdot}g^{-1}$ at pH 7, which is higher than that for any other kind of carbon (carbon nanotubes, nanoporous carbon, AC, carbon aerogel, carbon nanofibers) [6]. Sitko *et al.* [44] reported the Zn^{2+} maximum adsorption uptake of MGO at 346 $mg{\cdot}g^{-1}$ for a wide range of pH values (5 to 8). In contrast, Lee and Yang [45] observed a Zn^{2+} adsorption capacity on MGO of about 30 $mg{\cdot}g^{-1}$ at room temperature. The variability in results of Zn^{2+} adsorption uptake might be explained by the different amounts of MGO surface functional groups owing to the differences in preparation conditions. Indeed, the cation adsorption mechanism on MGO is mainly due to complexation with surface functional groups (chemisorption) and electrostatic interactions, but hydrogen bonding and hydrophobic interactions also play a role [37,46].

The hybrid CS/MGO material is claimed to be versatile with good mechanical properties, different kinds of adsorption sites (efficient toward cations and anions), eco-friendly (biodegradable and biocompatible) and easy to separate from an aqueous solution. The non-toxicity of the CS/MGO composite has been demonstrated by Samuel [47]. The affinity of CS/MGO hybrids toward anionic and cationic dyes is reported in several articles [37,48–50]. A lot of studies reported maximum adsorption uptake of about 100 or even several hundreds $mg{\cdot}g^{-1}$ for cationic metals such as Cu^{2+} [51,52], Pb^{2+} [14,40,51,53] Hg^{2+} [54] and Au^{3+} [14] on CS/MGO, depending on the temperature, the pH, the equilibrium time, the initial concentration of adsorbent and the composition of the CS/MGO hybrid. The adsorption capacities of a metal on the CS/MGO hybrid are sometimes reported to be higher (Q_{max} = 381 $mg{\cdot}g^{-1}$ for Hg^{2+}) [54] than on pure MGO (Q_{max} = 35 $mg{\cdot}g^{-1}$ for Hg^{2+}) [55]. Indeed, Liu *et al.* [14] showed that a CS/MGO composite (5 wt% of MGO) without crosslinking, had higher adsorption capacities (1076 $mg{\cdot}g^{-1}$ and 216 $mg{\cdot}g^{-1}$ for Au^{3+} and Pb^{2+}, respectively) than a composite prepared from cross-linked CS (990 $mg{\cdot}g^{-1}$ for Au^{3+} and 180 $mg{\cdot}g^{-1}$ for Pb^{2+}).

The adsorption of Zn^{2+} was reported on the hybrid imprinted polymer CS/MGO showing a maximum adsorption capacity close to 71 $mg{\cdot}g^{-1}$ [56]. To the best of our knowledge, the Zn^{2+} or MTP adsorption was never studied on CS/MGO composite. From literature, CS/MGO composites have an effective adsorption toward metal pollutants (both anions and cations) [57], but data concerning organic ions and metal cation–organic molecule mixture removal is limited. Thus, our aim was to study carefully the adsorption of a mixture of an organic pollutant (MTP) and a metal cation (Zn^{2+}) on CS/MGO composites.

For this purpose, pure and hybrid CS/MGO beads have been prepared with two different MGO mass contents (1.5 and 3 wt% in the precursor CS solution). The prepared beads were used to study the kinetics and adsorption isotherms of Zn^{2+} ions and MTP in water. In this paper, adsorption mechanisms are discussed and correlated to the bead's properties. The selectivity of the same CS/MGO beads toward a MTP-Zn^{2+} mixture is also discussed. The beads' regeneration and their efficiency after five cycles have been studied. The novelty of this work is the comparison of the hybrid CS/MGO beads prepared with two different MGO mass contents for the adsorption properties of two pollutants of different characteristics: a metallic cation (i.e., Zn^{2+}) and an organic one (i.e., MTP).

2. Materials and methods

2.1. *Chemicals*

The CS powder (deacetylation degree of 89%, molecular weight (M_W) 175,000 $g{\cdot}mol^{-1}$) was purchased from France CHITINE (Orange, France).

MGO was obtained by the Hummers method [58]: in brief, 10 g of graphite powder (Timrex® KS4 graphite, from IMERYS, Switzerland) was first mixed with 5 g of sodium nitrate (>99 wt%). In this mixture, 230 mL of sulphuric acid (95–97 wt%) was added slowly while maintaining the temperature below 5 °C. After homogenization, 30 g of potassium

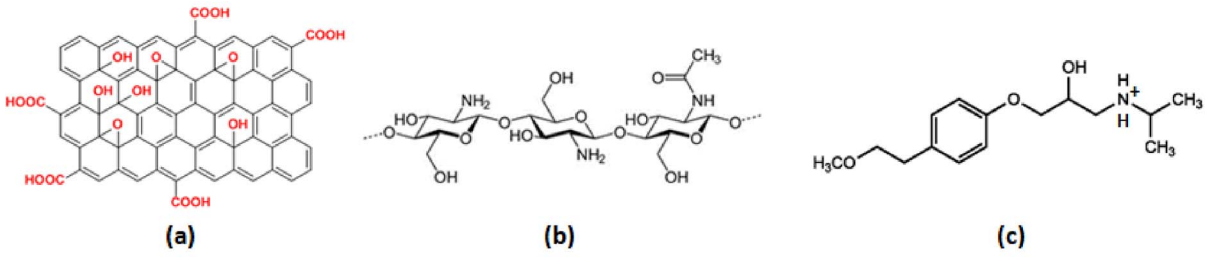

Figure 1. Molecular structure of (a) MGO, (b) CS and MTP at pH 6.5.

permanganate (>99 wt%) and 460 mL of distilled water were added. Finally, 80 mL of hydrogen peroxide (30 wt%) was added. After washing with distilled water, filtration, drying and grinding, the Multilayered Graphene Oxide (MGO) was obtained (Figure 1a).

Zinc chloride (>98 wt%) and MTP (>98 wt%) were purchased from Sigma-Aldrich. With pKa1/pKa2 values equal to 9.7/14 [59], MTP is in a cationic form at natural water pH (pH ≈ 6.5) (Figure 1c).

2.2. *Preparation and characterization of the beads*

2.2.1. *Hydrogel bead preparation*

Firstly, the synthesis of hybrid CS beads containing MGO powders was investigated (Figure 2). The CS powder was dissolved in a 0.5 mol·L^{-1} acetic acid solution to obtain a viscous solution of 2.1 wt% concentration. The MGO powder charge was dispersed at 3.2 wt% in the same volume of 0.5 mol·L^{-1} acetic acid using an ultrasonic probe (20 kHz, 1 h). Then the two solutions were mixed (CS and charges). Finally, small amounts of either CS powder or MGO powder were added step-by-step to get the desired 1.5 wt% or 3 wt% MGO concentration, respectively, in the mixture solution. The latter solution was stirred over 24 h before shaping the hybrid beads.

To shape the beads, the solution was passed through a 1.2 mm diameter syringe using a peristaltic pump at 20 mL·min^{-1}. The formed drops fell into a 10 wt% NaOH gelation bath, and 2 mm diameter hybrid CS beads having good size homogeneity and the required stability were obtained (Figure 2).

Prior to any use, the beads were washed under agitation in distilled water, until neutral pH was reached. The beads were either kept in distilled water to study their adsorption properties or freeze-dried for characterization purposes (gas adsorption, infrared spectroscopy). The freeze-drying included first a dipping step in liquid nitrogen then a vacuum step (1 Pa) to sublimate water.

Pure CS beads were prepared in the same way (Figure 2), from 3.5 wt% CS solution prepared in 0.5 mol·L^{-1} acetic acid. Three types of beads were thus studied: pure CS beads referred as 1-CS, and hybrid CS beads containing 1.5% of MGO (2-CS/1.5MGO) and 3% of MGO (2-CS/3MGO). The chitosan powder is referred as CS.

2.2.2. *Characterization*

The chemical composition was determined by elemental analysis (CHONS-FLASH2000, Thermo Scientific). In order to determine the surface groups and surface charge of the raw materials, potentiometric titrations were performed with an automatic titration instrument (Titrino Plus, METROHM). Samples (100 mg of CS or MGO powders) were dispersed in 75 mL of a 0.01 mol·L^{-1} sodium nitrate solution and stirred for 48 h. Then pH was adjusted to 3 by adding a controlled amount of HCl (0.1 mol·L^{-1}) and titration was performed using 0.1 mol·L^{-1} NaOH solution.

To identify the interactions between CS and MGO, infrared absorption spectra were recorded with a Nicolet 6700 Thermo Scientific Spectrometer. The FTIR spectra of raw material and beads (dried and crushed) were obtained using the transmission mode. Dried KBr and 2–10 wt% of sample were mixed and ground. 100 mg of the ground mixture was compressed under 10 tons/cm^2 pressure to obtain pellets. The spectra were recorded using an average of 128 scans with a resolution of 4 cm^{-1}.

The morphology of MGO was observed with a Philips CM20 Transmission Electron Microscope

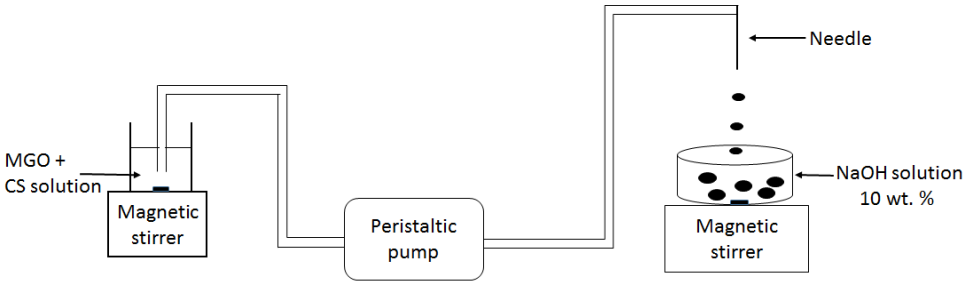

Figure 2. Schematic representation of the chitosan/hybrid beads synthesis method.

(TEM). The porous texture of the hybrid materials was characterized by scanning electronic microscopy using a Cryo-SEM (S4500HITACHI). After immersion in liquid nitrogen at −196 °C, the beads were fractured and introduced in a transfer chamber, then ice was sublimated at −70 °C under vacuum (10^{-3} Pa) in order to preserve the porous network free of water, allowing its observation.

Powder X-ray diffraction (XRD) of MGO was recorded with a Thermo Electron ARL'XTRA diffractometer equipped with a Cu anode and Si(Li) solid-state detector, to measure the d_{001} interlayer distance of MGO.

Nitrogen adsorption–desorption experiments at 77 K (ASAP 2020, Micromeritics) were performed to determine the BET specific surface areas (P/P_0 ranging from 0.05 to 0.3) of the powdered samples and freeze-dried beads after degassing under vacuum (0.26 mPa, 80 °C, 72 h to avoid any degradation of CS).

The raw materials and the prepared beads were analysed by TGA (heating rate of 10 °C·min^{-1}) under a nitrogen flow (1 L·h^{-1}). The amount of water and of each component in the beads (i.e., CS and MGO) was thus quantified.

2.3. *Adsorption studies*

The adsorption kinetics of 1.5 mmol·L^{-1} solutions of $ZnCl_2$ and MTP were conducted at 25 °C and pH 6.5 (adjusted with NaOH or HCl if necessary), using 200 mg of single adsorbent in 100 mL of solution. Ultra-pure water (σ_{water} = 0.055 µS·cm^{-1}) was used as solvent. Samples of 0.1 mL (Zn^{2+}) or 0.5 mL (MTP) were taken out from the solution at different times between 2 min and 48 h. The MTP concentration was followed by UV spectroscopy (Cary100, Agilent) at 229 nm. The Zn^{2+} concentration was analysed by atomic absorption spectroscopy (Z-8100, Hitachi). Calibration curves were established in the range of 0.2–1.2 mg·L^{-1} (λ = 213.9 nm, detection limit: 0.008 mg·L^{-1}).

The kinetic experimental curves were fitted by the pseudo-first-order (1) and pseudo-second-order (2) models:

$$Q(t) = Q_m \cdot (1 - e^{-k_1 t}) \quad (1)$$

$$Q(t) = \frac{k_2 \cdot Q_m^2 \cdot t}{1 + (k_2 \cdot Q_m \cdot t)} \quad (2)$$

where $Q(t)$ (mmol·g^{-1}) is the adsorbed amount as a function of time (t), Q_m is the maximum adsorbed amount (mmol·g^{-1}) in the experimental conditions, k_1 (min^{-1}) and k_2 (g·mmol^{-1}·min^{-1}) are the velocity constants for the first-order and second-order equations, respectively.

The adsorption isotherms were studied by adding 20 mg of CS beads or 5 mg of hybrid CS/MGO beads in 100 mL of pollutant solution at different concentrations (0.2–2 mmol·L^{-1}). After six days of orbital agitation (175 rpm, room temperature), the solutions were filtered and analysed by UV–visible or atomic absorption spectroscopy. The experimental isotherms were fitted using the Langmuir equation (3), the Freundlich equation (6) and the Langmuir–Freundlich equation (7):

$$Q_e = \frac{Q_{max} \cdot K_L \cdot C_e}{1 + (K_L \cdot C_e)} \quad (3)$$

where Q_e is the equilibrium pollutant amount adsorbed on sorbent (mmol·g^{-1}). Q_e was calculated according to the following equation:

$$Q_e = \frac{(C_0 - C_e) \times V}{m} \quad (4)$$

where C_0, C_e are the initial and equilibrium concentrations of pollutant (mmol·L^{-1}) respectively, V is the solution volume (L), m is the adsorbent weight (g), Q_{max} the maximum adsorption capacity

of the sorbent (mmol·g^{-1}) and K_L is the Langmuir adsorption constant (L·mmol^{-1}) used in (3). The Langmuir model assumes that adsorption takes place at uniform energy sites on the surface of the adsorbent, adsorption being rather considered monolayered. The Freundlich isotherm model assumes a multilayered adsorption on a heterogeneous adsorbent surface with different energy sites.

The separation factor (R_L) was also calculated as follows:

$$R_L = \frac{1}{1 + K_L \cdot C_e} \tag{5}$$

where R_L indicates if the adsorption process is favored or not. The adsorption is irreversible if $R_L = 0$, favorable if $0 < R_L < 1$ and unfavorable for $R_L = 1$.

$$Q_e = K_F \cdot C_e^{1/n}. \tag{6}$$

In (6), K_F (L·g^{-1}) and n are the Freundlich adsorption constants indicating the extent of the adsorption (relative adsorption capacity), and the degree of nonlinearity between the amount of adsorbed pollutant and the pollutant concentration in the solution, respectively.

$$Q_e = \frac{Q_{\max}(K_{\mathrm{LF}} \cdot C_e)^b}{1 + (K_{\mathrm{LF}} \cdot C_e)^b}. \tag{7}$$

In (7), K_{LF} (L·mmol^{-1}) and b are the Langmuir–Freundlich adsorption constants. The quality of the adjustment procedure was given by the R^2 correlation coefficient.

In order to evaluate the adsorption efficiency sites, and to compare the adsorption ability of the raw material and the hybrid material, the number of the theoretically available adsorption sites was calculated considering the mass of each material within the hybrid beads. For this calculation, the total adsorption amount is assumed to be the sum of the adsorption uptake of each component in the hybrid system. These values were compared to the measured adsorption capacity to obtain the percentage of occupied active sites.

2.4. *Study of adsorption selectivity between Zn^{2+} and MTP*

In order to study the adsorption selectivity of the beads towards organic and inorganic cations, a kinetic study was carried out using the more homogeneous beads (2-CS/1.5MGO) as adsorbent in an equimolar mixture of MTP and Zn^{2+}. Precisely, 200 mg of beads were added to 100 mL of a MTP-Zn^{2+} equimolar mixture solution with a total initial concentration ([Zn^{2+}] + [MTP]) set at 0.75 mmol·L^{-1}, 1.5 mmol·L^{-1} and 2 mmol·L^{-1} to evaluate the competition effects. The three kinetics were studied at room temperature and at pH 6.5, under magnetic stirring at a 250 rpm constant speed.

2.5. *Study of the bead's regeneration*

The 2-CS/1.5MGO beads loaded with MTP and Zn^{2+} were selected for the regeneration studies. An adsorption–desorption cycle was repeated five times. Firstly, MTP or Zn^{2+} adsorption was conducted using 100 mg of beads in 100 mL of 1 mmol·L^{-1} pollutant solution, at room temperature and pH 6.5. After 48 h magnetic stirring (250 rpm), the adsorbed pollutant amount (n_{ads}) was calculated using (8):

$$n_{\mathrm{ads}} = (C_0 - C_f) * V \tag{8}$$

where C_0 and C_f are the initial and final concentrations of the pollutant in the solution (mmol·L^{-1}), measured by UV–visible or atomic absorption spectroscopy and V (L) the volume of the solution.

Then the beads were separated from the pollutant solution and rinsed with distilled water. For the regeneration step, beads were added to a 100 mL HCl solution at pH 4 and kept under stirring (250 rpm) at room temperature for 72 h. The amount of desorbed pollutant (n_{des}) was then determined using (9).

$$n_{\mathrm{des}} = (C_{rf} - C_{r0}) * V \tag{9}$$

where C_{r0} and C_{rf} are the concentrations (mmol·L^{-1}), measured by UV–visible or atomic absorption spectroscopy at the beginning and at the end of the regeneration step and V the volume of the solution.

Finally, the regeneration percentage (R,%) was calculated using (10).

$$R\% = \left(\frac{n_{\mathrm{des}}}{n_{\mathrm{ads}}}\right) * 100. \tag{10}$$

3. Results and discussion

3.1. *Characterization of the hybrid beads and their components: CS and MGO*

MGO shows an acidic pH_{ZC} of 3.2 due to the large amount of acidic oxygenated functional groups generated during its synthesis while a strong oxidation

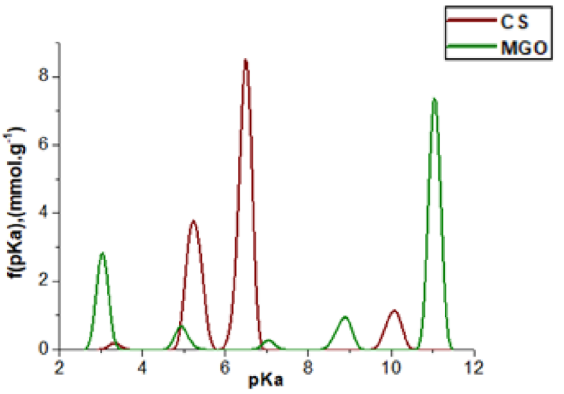

Figure 3. pKa value and amount of functional groups (mmol·g^{-1}) of CS and MGO raw material.

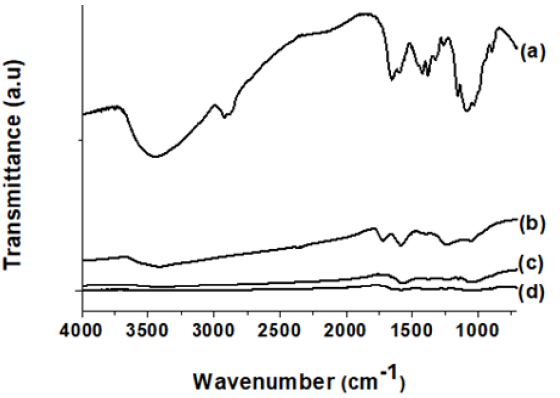

Figure 4. FTIR spectra of (a) CS, (b) MGO, (c) 2-CS/1.5MGO and (d) 2-CS/3MGO.

Table 1. Chemical composition and surface functional groups of CS powder and MGO

Material		CS powder	MGO
Chemical composition (wt%)	O	37.0	33.0
	C	42.3	56.2
	H	7.1	2.1
	N	7.4	0.0
	S	0.0	0.7
	pH_{ZC}	9.6	3.2
Functional groups (mmol·g^{-1})	$3 < pK_a < 7$	5.0	1.4
	$7 < pK_a < 11$	0.5	3.1
	Total	5.5	4.5

of graphite occurs. The total amount of acidic oxygenated groups is ~4.5 mmol·g^{-1}. Parts of them are carboxylic groups (1.4 mmol·g^{-1}) but most of them are phenolic-type groups having a high pK_a (11). The presence of such acidic groups boosts MGO's ability to adsorb cationic species through electrostatic interactions. Indeed, at pH 6.5 only carboxylic functions are deprotonated and appear as anionic groups. Two types of carboxylic groups having pK_a values of 3 and 5 are quantified at 1 and 0.4 mmol·g^{-1} respectively (Figure 3).

CS shows a basic pH_{ZC} of 9.6 due to the large amount of amine functional groups generated by the deacetylation process of the chitin precursor. The total amount of CS functional-groups is around 5 mmol·g^{-1}. CS surface functionality includes mainly oxygenated groups and NH_3^+ groups capable of adsorbing anionic species through electrostatic interactions and to interact with cations through nitrogen doublets forming chelating bonds [24]. In addition, the CS chains include 5 mmol·g^{-1} of NH_2 (calculated from the length of the chains $Mw = 175$ kg·mol^{-1} and the deacetylation degree 0.89). At pH 6.5, only half of the amine groups are protonated, thus CS includes 2.5 mmol·g^{-1} of NH_3^+ groups and 2.5 mmol·g^{-1} of NH_2 groups.

The raw CS and MGO are both oxygen-rich materials as evidenced by their elemental analyses (Table 1, O content > 30 wt%). CS possesses a relatively high amount of nitrogen (7 wt%) in agreement with the amine and amide presence on the polysaccharide polymer skeleton. The carbon atoms (56 wt%) in MGO belong to the graphene sheets. The hydrogen atoms (2.1 wt%) are included in hydroxyl, carboxylic and phenolic surface groups. The traces of sulfur (0.7 wt%) correspond to sulfuric acid residues, originating from the MGO preparation process. For CS and MGO, the total amount CHONS elements is less than 100% which can be explained by the presence of material impurities including some minerals.

FTIR analyses were carried out to confirm the MGO synthesis and to ensure that the MGO spectrum (Figure 4b) and its characteristic bands (Table 2) are comparable to the reported ones.

MGO possesses typical bands: OH groups at 1397 and 3419 cm^{-1}, C–O of acids, alcohols, phenols, ethers and esters groups at 1050 cm^{-1}, C=O of the carboxylic acid and carbonyl groups at

Table 2. FTIR characteristic bands of CS, MGO and CS/MGO beads

Assignment	Wavenumber (cm^{-1})		
	CS [25,60]	MGO [37,54]	CS/MGO
υ(C–O, C–O–C) (polysaccharide skeleton)	898, 1026, 1081 and 1152	-	898, 1070, 1150
υN–H(NH_2), υ(N–H)	1422	-	1422
υN–H (amide)	1653	-	1653
υ(C–H)	2850, 2890	-	2850, 2890
υ(C–CH_3)	1384	-	
υC–CH_2 asymmetric banding	1418	-	
υC–OH	1259	-	
υO–H, N–H	3400	1397	1384
		3419	3417
υC=O (carboxyl)	-	1717	1717
υC=C	-	1570	1575
υC–O (epoxy)	-	1230	1235
υC–O (carbonyl, carboxyl)		1050	

1717 and 1230 cm^{-1} and C=C of the graphene planes at 1570 cm^{-1}.

FTIR analyses were performed on the hybrid beads in order to prove that the MGO previously incorporated into the CS solution had been successfully transferred into the beads. The CS FTIR spectrum (Figure 4a) displays the well-known peak signature of the CS skeletons at 898 and 1152 cm^{-1} corresponding to stretching bands of the polysaccharide skeleton (C–O and C–O–C bonds) [60]. The band at 1259 cm^{-1} is attributed to the alcohol (OH) group's stretching band, the 1384 cm^{-1} band to the CH_3 asymmetric bending and the 1418 cm^{-1} band to the C–N axial vibrations and N–H angular bending. The bending vibrations of NH_2 groups appear at 1422 cm^{-1}.

The vibration of acetamide groups appears at 1653 cm^{-1}, the stretching modes of C–H bonds at 2850 and 2890 cm^{-1} and the vibration of amine and hydroxyl groups is observed at 3400 cm^{-1}.

The IR spectra of the CS/MGO hybrid beads (Figure 4c, d) display mainly the bands of CS because of the low amount of MGO in the blended materials and the high intensity of the CS IR bands.

TEM observations show the MGO morphology (Figure 5a) as a stacked multi-layer planar graphene oxide comprising three to eight stacked layers [61]. The 001 reflection peak observed by XRD analysis at $2\theta K_\alpha$Cu = 13.3°, corresponds to a d_{001} = 0.6 nm mean interlayer value. Additionally, from the half-height width of this reflection (2°), an average of six randomly stacked graphene-oxide layers is calculated according to the Scherrer equation.

According to the cryo-SEM images, the 1-CS beads (Figure 5b) and 2-CS/1.5MGO (Figure 5c) hybrid beads are observed to be relatively homogeneous. The presence of non-dispersed MGO aggregates (4 μm approximate size) in 2-CS/3MGO (Figure 5d) beads show that they are less homogeneous than 2-CS/1.5MGO indicating a limited dispersion of MGO in the CS gel.

The water mass loss is observed by TGA in the range 25 °C–225 °C. The higher the MGO loading content, the lower the water content within the beads (Table 3). Between 250 °C and 400 °C the decomposition of CS and MGO is observed. The mass losses show that the hydrogel beads contain 86–90 wt% of water. The 2-CS/1.5MGO and the 2-CS/3MGO hybrid beads contain approximately 10 wt% and 14 wt% of solid mixture, respectively. As the CS and MGO thermal decompositions occur simultaneously, the determination of the CS and MGO relative amounts is not accurate using TGA analysis.

One of the expected benefits of preparing hybrids with CS is to increase the porosity. Indeed, the raw CS powder has a BET specific surface area of 2 $m^2 \cdot g^{-1}$

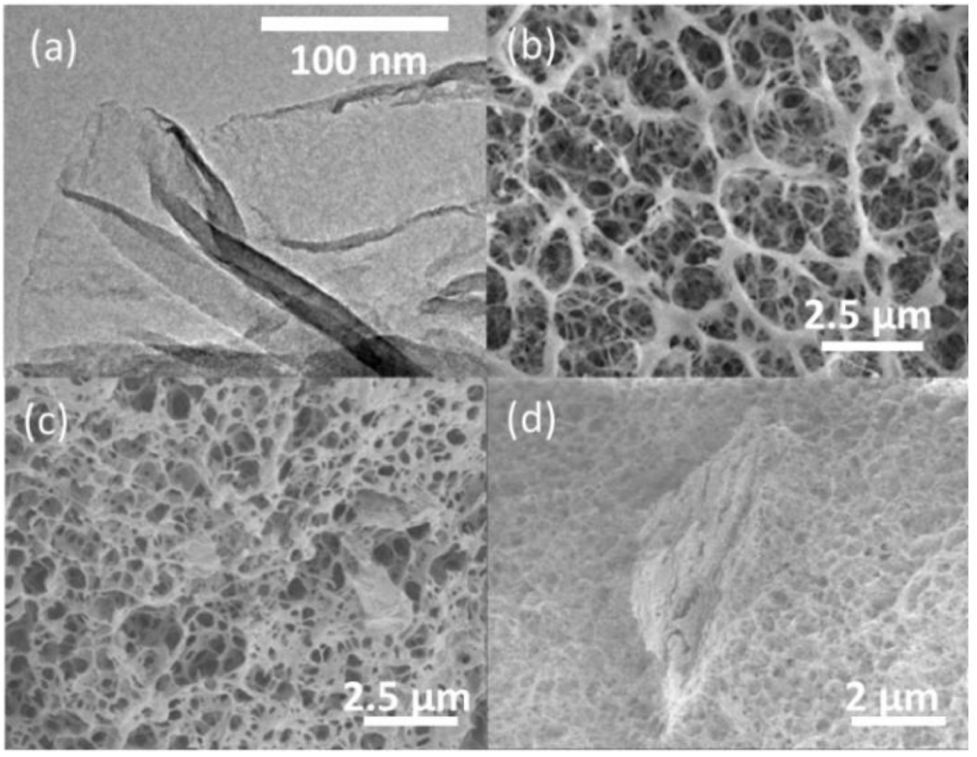

Figure 5. TEM images (×15,000) of MGO (a), Cryo-SEM (×5000) of 1-CS (b), 2-CS/1.5MGO (c) and 2-CS/3MGO (d).

Table 3. Water content and mass of active material in raw material and in hydrogel beads measured by TGA and their BET specific surface areas

Material	1st mass loss $\Delta m/m$ (%)* $25 < T$ (°C) < 225	2nd mass loss $\Delta m/m$ (%)** $250 < T$ (°C) < 400	S_{BET} ($m^2 \cdot g^{-1}$)
CS	6	66	2
MGO	17	32	38
1-CS	90	3	35
2-CS/1.5MGO	89	4	67
2-CS/3MGO	86	4	33

*The first mass loss corresponds to the water content, **the second mass loss corresponds to CS and MGO degradation.

while the freeze-dried beads are much more porous (S_{BET} = 35 $m^2 \cdot g^{-1}$, Table 3).

The S_{BET} of 2-CS/1.5MGO freeze-dried beads (67 $m^2 \cdot g^{-1}$) is almost twice that of pure CS beads. However, the increase in the MGO proportion leads to the formation of more compact and less porous 2-CS/3MGO beads explaining their S_{BET} reduction (33 $m^2 \cdot g^{-1}$).

3.2. *Kinetics adsorption study*

3.2.1. *Zn^{2+} adsorption kinetics*

Zn^{2+} ions are known to be adsorbed by chelation on CS thanks to the non-binding oxygen and nitrogen doublets of the hydroxyl and amino groups. Using the kinetic study condition, 21% of the Zn^{2+} initial amount was adsorbed by the powdered CS

Table 4. Kinetics parameters of the model fitting for the adsorption of Zn^{2+} and MTP on the CS, MGO and hydrogel beads

Adsorbent	Kinetics model*	Zn^{2+}			MTP		
		Kinetics parameters			Kinetics parameters		
			k_1 (min^{-1})			k_1 (min^{-1})	
		R^2	k_2 ($g{\cdot}mmol^{-1}{\cdot}min^{-1}$)	Q_m ($mmol{\cdot}g^{-1}$)	R^2	k_2 ($g{\cdot}mmol^{-1}{\cdot}min^{-1}$)	Q_m ($mmol{\cdot}g^{-1}$)
CS	1st	0.94	0.14 ± 0.1	0.16 ± 0.01	0.97	1 ± 0.0	$9.3 \times 10^{-6} \pm 2 \times 10^{-7}$
	2nd	0.91	2 ± 1	0.17 ± 0.02	0.98	0.05 ± 0.02	$9.7 \times 10^{-6} \pm 2 \times 10^{-7}$
MGO	1st	0.98	0.9 ± 0.1	0.670 ± 0.005	0.76	0.07 ± 0.02	0.51 ± 0.03
	2nd	0.99	3.4 ± 0.4	0.679 ± 0.003	0.88	0.20 ± 0.05	0.55 ± 0.02
1-CS	1st	0.97	0.8 ± 0.1	0.097 ± 0.002	0.85	$0.026 \pm 5 \times 10^{-3}$	$0.0051 \pm 4 \times 10^{-4}$
	2nd	0.97	19 ± 6	0.099 ± 0.002	0.83	6 ± 2	$0.0058 \pm 5 \times 10^{-4}$
2-CS/1.5MGO	1st	0.98	0.012 ± 0.001	0.280 ± 0.007	0.98	$164 \times 10^{-4} \pm 6 \times 10^{-4}$	0.212 ± 0.002
	2nd	0.97	0.048 ± 0.008	0.30 ± 0.01	0.98	$105 \times 10^{-3} \pm 7 \times 10^{-3}$	0.228 ± 0.003
2-CS/3MGO	1st	0.95	0.016 ± 0.002	0.47 ± 0.02	0.97	$97 \times 10^{-4} \pm 5 \times 10^{-4}$	0.518 ± 0.006
	2nd	0.99	0.038 ± 0.004	0.53 ± 0.01	0.99	$248 \times 10^{-4} \pm 7 \times 10^{-4}$	0.558 ± 0.003

*Kinetic model, 1st: pseudo-first-order, 2nd: pseudo-second-order.

(Q_m = 0.16 $mmol{\cdot}g^{-1}$ = 10 $mg{\cdot}g^{-1}$) indicating a 6.4% occupation rate for the NH_2 sites. The low Q_m value compared to the NH_2 available site concentration (2.5 $mmol{\cdot}g^{-1}$) is explained by the diffusion limitation of adsorbate in the CS particles because of the low accessibility of the adsorption site.

Pure CS beads are less effective than CS powder, as 13% of the initial amount of Zn^{2+} was adsorbed corresponding to 4% of NH_2 sites (Q_m = 0.1 $mmol{\cdot}g^{-1}$ = 6.5 $mg{\cdot}g^{-1}$). The decrease in the number of occupied sites compared to powdered CS is attributed to the sites' consumption owing to the intermolecular interactions within the polymer chains after the beads' coagulation.

Table 4 indicates that the Zn^{2+} adsorption kinetics of the CS powder (CS) and CS hydrogel beads (CS-1) are better fitted by a first-order model as R^2 value is closer to one (Table 4). The kinetic constants in Table 4 shows that the adsorption is at least four times faster in the beads than in raw CS owing to a higher porosity and a higher exchange surface.

Zn^{2+} adsorption on the MGO powder is very fast in comparison with adsorption on the CS powder. For adsorption of Zn^{2+} on MGO, both first- and second-order models fit well the experimental data (Table 4). Ninety one percent of the Zn^{2+} initial amount is adsorbed onto raw MGO (Q_m = 0.68 $mmol{\cdot}g^{-1}$ = 44.5 $mg{\cdot}g^{-1}$). The high affinity of Zn^{2+} to MGO is attributed to electrostatic interactions with the carboxylic groups. By assuming a chelation by the carboxylic acid, 49% of the MGO carboxylic groups would be occupied.

The kinetic curves and adsorption data (Figure 6, Table 4) show that both models (first- and second-order models) are possible for describing 2-CS/1.5MGO kinetics whereas the pseudo-second-order model is the most reliable one for 2-CS/3MGO. Using the second-order model, the kinetics constant is higher for 2-CS/1.5MGO than for 2-CS/3MGO suggesting that the Zn^{2+} transfer towards the adsorption sites is faster as the S_{BET} reaches a high value (67 $m^2{\cdot}g^{-1}$ for 2-CS/1.5MGO in comparison with 33 $m^2{\cdot}g^{-1}$ for 2-CS/3MGO) and the MGO amount is low (1.5%). The presence of MGO enhances the adsorption sites accessibility for Zn^{2+}, suggesting that the pseudo-second-order model better fits the kinetic data.

Figure 6 shows that 2-CS/1.5MGO (Q_m = 18 $mg{\cdot}g^{-1}$) and 2-CS/3MGO ($Q_m \approx$ 34.6 $mg{\cdot}g^{-1}$) beads are three times and five times more effective for zinc adsorption than the CS beads, respectively. Globally, 13% of the beads' sites (amino + hydroxyl groups of CS + carboxylic groups of MGO) were occupied in 2-CS/1.5MGO and 27% in 2-CS/3MGO.

Assuming that adsorption on the two components (CS and MGO) in the hybrid material is purely

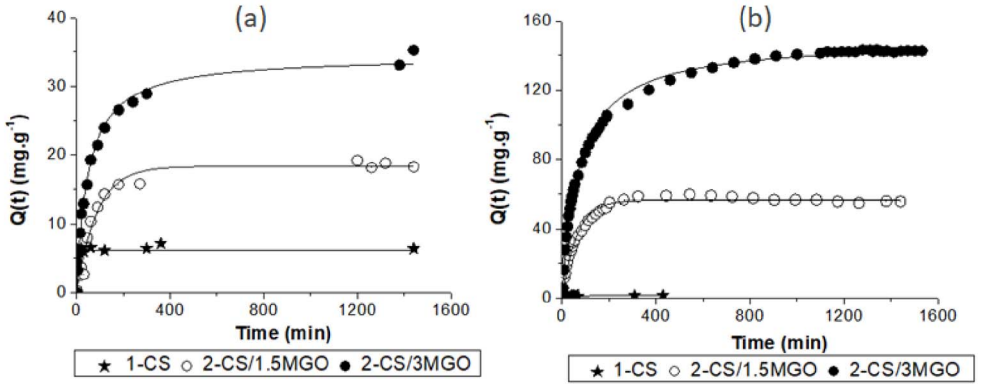

Figure 6. Adsorption kinetics of pure and hybrid hydrogel CS beads towards Zn^{2+} (a) and MTP (b). The continuous lines represent calculated data using the best-fitting model.

additive, the adsorbed amounts of zinc by CS in the 2-CS/1.5MGO and 2-CS/3MGO beads were estimated by taking into account the mass proportion of each component. According to this calculation, the zinc adsorption uptakes by CS were estimated to be 0.07 mmol·g^{-1} and 0.05 mmol·g^{-1} in the 2-CS/1.5MGO and 2-CS/3MGO beads, respectively. Moreover, 45% of the available MGO carboxylic sites could be occupied by Zn^{2+} in 2-CS/1.5MGO and 69% in 2-CS/3OG.

These results show that MGO is very effective for Zn^{2+} removal even when mixed with CS and its COO^- sites are accessible for providing electrostatic interactions with these cations. The MGO behaves in a way similar to an ion exchange resin, suggesting the possibility of its regeneration in an acidic environment.

3.2.2. *Metoprolol adsorption kinetics*

CS powder and CS beads have a low MTP adsorption capacity. Only 1.2% (Q_m = 0.009 mmol·g^{-1} = 2.5 mg·g^{-1}) and 0.8% (Q_m = 0.006 mmol·g^{-1} = 1.5 mg·g^{-1}) of the MTP initial amount is adsorbed by powdered CS and CS beads, respectively. These low MTP uptakes are explained by repulsions between the adsorbent and the adsorbate owing to the positive charge of CS. The interactions between MTP and CS could be hydrogen bonding between CS amine and hydroxyl groups. The decrease in the beads' adsorption capacity compared to the powder could be explained by the unavailability of the NH_2 and OH sites which are involved in hydrogen bonding between the polymer chains within the beads. As MTP adsorption on CS powder and on CS beads is very low, the comparison and discussion of the simulated kinetics data appear difficult.

As expected, MGO is very effective towards MTP adsorption thanks to its negatively charged surface. Seventy three percent of the MTP initial amount is adsorbed at a 0.55 mmol·g^{-1} adsorption uptake (147 mg·g^{-1}). Mainly electrostatic interactions are responsible for the binding between MTP and MGO but the quantification of the two contributions is not possible. Assuming that MTP is mainly adsorbed by electrostatic bonds on carboxylic sites, approximately 40% of these MGO sites would be occupied.

The adsorption kinetics of MTP on MGO powder is better fitted by a second-order model (Table 4) in agreement with the different types of MGO anionic sites. MGO adsorption sites are well accessible for MTP molecules as the kinetic constant for adsorption on MGO is higher than that for adsorption on hybrid beads 2-CS/1.5MGO and 2-CS/3MGO (Table 4). Both the first and the second-order models can fit the MTP adsorption kinetics by 2-CS/1.5MGO and 2-CS/3MGO beads (Table 4).

The blending of MGO with CS yields efficient hybrid materials such as 2-CS/1.5MGO (Q_m = 0.23 mmol·g^{-1} = 61 mg·g^{-1}) and 2-CS/3MGO (Q_m = 0.56 mmol·g^{-1} = 149 mg·g^{-1}) beads which adsorb 35 and 100 times more than pure CS beads (Figure 6), respectively. The adsorption mechanism of MTP by materials including MGO may be also explained by chemisorption (electrostatic) on MGO. Assuming that CS is almost inert with respect to MTP and that adsorption mechanism involves

only the carboxylic sites, therefore 50% and 80% of these sites would be occupied in 2-CS/1.5MGO and 2-CS/3MGO, respectively. The high ratio of the occupied adsorption sites illustrates the good accessibility to the MGO sites within the hybrid beads. The MGO incorporation to CS brings anionic adsorption sites, as well as a good accessibility to these adsorption sites thanks to the porosity improvement of the beads (Table 3). However, the MTP adsorption kinetics are faster (Table 4) for pure MGO than for MGO–CS blended hybrids. The mixing of MGO with an inert CS matrix has the effect to slow down the MTP diffusion through the beads, thus moderating its adsorption kinetic.

3.2.3. *Beads' selectivity*

Because Zn^{2+} and MTP pollutants may coexist in wastewater, the simultaneous adsorption of the two species were studied. Adsorption kinetics of an equimolar mixture of Zn^{2+} and MTP on 2-CS/1.5MGO beads were studied at total pollutant initial concentrations ($[Zn^{2+}] + [MTP]$) of 0.75, 1.5 and 2 mmol·L^{-1} as reported in Figure 7. The fitted kinetics parameters are listed in Table 5.

According to Table 5, the second-order model better fits the experimental kinetics whatever the pollutant (MTP or Zn^{2+}) and the initial concentrations. The kinetics constant rates for MTP ions are increasing together with initial concentration (Table 5). This is in agreement with MTP adsorption kinetics controlled by diffusion into the hybrid beads. By contrast the kinetics constant rates for Zn^{2+} ions decrease with increasing concentrations. This unexpected result might be related to the presence of various adsorption sites with various affinities for Zn^{2+} and showing different adsorption kinetics on MGO and CS sites. The kinetics on MGO sites could be quicker than on CS sites as previously observed (Table 4). Thus, at low concentration (0.75 mmol·L^{-1}), the MGO sites could be preferentially occupied by Zn^{2+}, and at concentrations higher than 1.5 mmol·L^{-1}, the Zn^{2+} could be also adsorbed on CS sites through chelation by CS amine groups.

Figure 7 shows that almost the same amounts (0.10–0.12 mmol·g^{-1}) of MTP and Zn^{2+} are adsorbed at an initial concentration of 0.75 mmol·L^{-1}. But on progressively increasing the initial concentration up to 2 mmol·L^{-1}, a MTP adsorption uptake stabilization (at about 0.12 mmol·g^{-1}) is observed as well as an increase in the Zn^{2+} uptake reaching about 0.3 mmol·g^{-1} (Table 5).

The adsorbed MTP amount for the 1.5 mmol·L^{-1} and 2 mmol·L^{-1} initial concentrations are quite similar (Figure 7), because the MTP adsorption sites are saturated or unavailable while Zn^{2+} ions adsorption uptake still increases with the initial concentration as their adsorption sites are still available. This could be related to a competition effect between the MTP and Zn^{2+} adsorption sites in these conditions. The adsorption competition between MTP and Zn^{2+} could occur on MGO sites (electrostatic interactions between cations and MGO carboxylic groups). The Zn^{2+} is expected to have a higher interaction energy with the MGO sites than with MTP because of its divalent charge compared to the single one of MTP cation.

For a 1.5 mmol·L^{-1} concentration, and a single adsorption on 2-CS/1.5MGO beads, only 37% and 30% of the Zn^{2+} and MTP initial amounts are adsorbed, respectively. In comparison, at the same concentrations in an equimolar adsorbate mixture (Figure 7), 70% and 38% of the Zn^{2+} and MTP initial amounts are adsorbed, respectively. Thus, a synergistic adsorption effect is observed for the mixture leading to higher uptakes despite the coexistence of two types of pollutants which can compete on some adsorption sites.

3.2.4. *Conclusion on the adsorption kinetics*

In terms of adsorption capacity, the beads containing MGO are more effective than pure CS ones. Indeed, the MGO brings new accessible and active adsorption sites for both Zn^{2+} and MTP. In addition, for 2-CS/1.5MGO beads, the increase in porosity in comparison with 1-CS beads allows an improved adsorbate transfer and a greater adsorption capacity. For all adsorbates, despite the increase in adsorption capacity together with the MGO loading ratio, the adsorption speed should depend on the accessibility to the CS and MGO adsorption sites by diffusion within the beads (Table 4). This accessibility is also related to the porosity.

Moreover, the number of oxygenated sites of pure MGO occupied by Zn^{2+} is greater than the number of MTP-occupied sites due to MTP's larger size. In MGO-loaded CS beads, MTP is adsorbed in the same range as Zn^{2+}, showing the important adsorption role of the two components: MGO and CS.

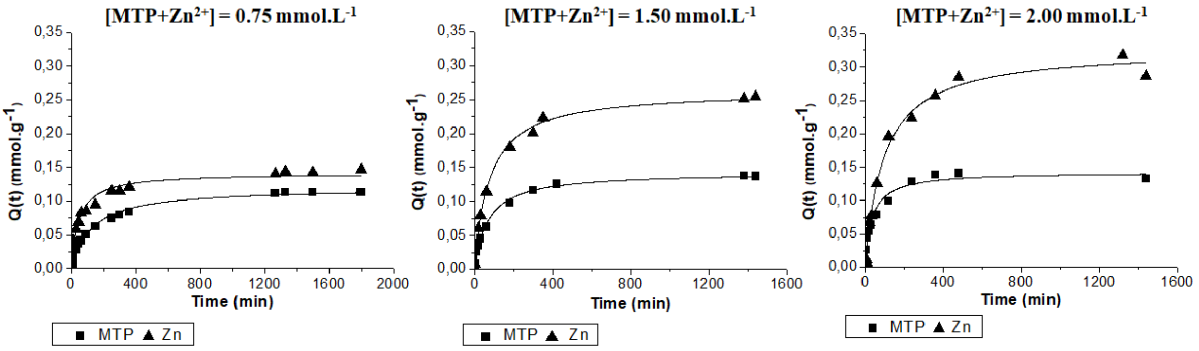

Figure 7. Adsorption kinetics of MTP and Zn^{2+} on 2-CS/1.5MGO beads in an MTP-Zn^{2+} equimolar mixture at different initial concentrations. The continuous lines represent calculated data using the best-fitting model.

Table 5. Kinetics parameters of the model fitting for adsorption of MTP and Zn^{2+} on 2-CS/1.5MGO beads at various initial MTP-Zn^{2+} equimolar concentrations

[MTP + Zn^{2+}] i^* (mmol·L^{-1})	Kinetics model**	Zn^{2+}			MTP		
		Kinetics parameters			Kinetics parameters		
			K_1 (min^{-1})			K_1 (min^{-1})	
		R^2	K_2 (g·$mmol^{-1}$·min^{-1})	Q_m (mmol·g^{-1})	R^2	K_2 (g·$mmol^{-1}$·min^{-1})	Q_m (mmol·g^{-1})
0.75	1st	0.90	0.016 ± 0.003	0.130 ± 0.005	0.96	0.0058 ± 0.0006	0.109 ± 0.003
	2nd	0.97	0.15 ± 0.02	0.142 ± 0.004	0.99	0.065 ± 0.006	0.120 ± 0.003
1.5	1st	0.97	0.010 ± 0.002	0.235 ± 0.009	0.97	0.011 ± 0.002	0.129 ± 0.005
	2nd	0.99	0.051 ± 0.004	0.263 ± 0.004	0.99	0.10 ± 0.01	0.143 ± 0.003
2	1st	0.98	0.008 ± 0.001	0.29 ± 0.01	0.93	0.020 ± 0.004	0.131 ± 0.006
	2nd	0.99	0.032 ± 0.005	0.33 ± 0.01	0.97	0.20 ± 0.04	0.143 ± 0.006

*Initial concentration of MTP and Zn^{2+} (mmol·L^{-1}), **kinetics model 1st: pseudo-first-order, 2nd: pseudo-second-order.

The Zn^{2+} and MTP adsorption on raw material (CS and MGO) occurs faster than on hybrid beads as far as adsorption sites are more directly accessible on the raw adsorbents.

The adsorption kinetic constants are in agreement with the MGO amount introduced into the hybrid beads: the higher the MGO content, the lower the porous surface area generated into the bead network and therefore the lower the adsorption kinetics.

3.3. *Adsorption isotherms*

3.3.1. *Simulation of experimental isotherms*

Figure 8 represents the adsorption isotherms at 25 °C of Zn^{2+} (a) and MTP (b) by the pure CS and the hybrid CS beads. The calculated adsorption capacities and adsorption parameters are given in Table 6. As shown in Figure 8a, b, regardless of the cationic adsorbate type (MTP or Zn^{2+}), adsorption capacities are higher for 2-CS/3MGO made at a higher MGO loading rate. This result demonstrates the great importance of MGO in the hybrid material for MTP and Zn^{2+} adsorption, MGO being more efficient than CS.

3.3.2. *Interpretation of Zn^{2+} adsorption isotherms*

Zn^{2+} adsorption isotherms on pure CS beads and on the CS/MGO hybrid beads, 2-CS/1.5MGO and 2-CS/3MGO, are better fitted by the Langmuir–Freundlich models with adsorption capacities of 40, 109 and 236 mg·g^{-1}, respectively (Table 6). Despite a quite moderate Q_m value found on pure CS beads, the R_L value (between 0 and 1) suggests a spontaneous adsorption of Zn^{2+} on CS through

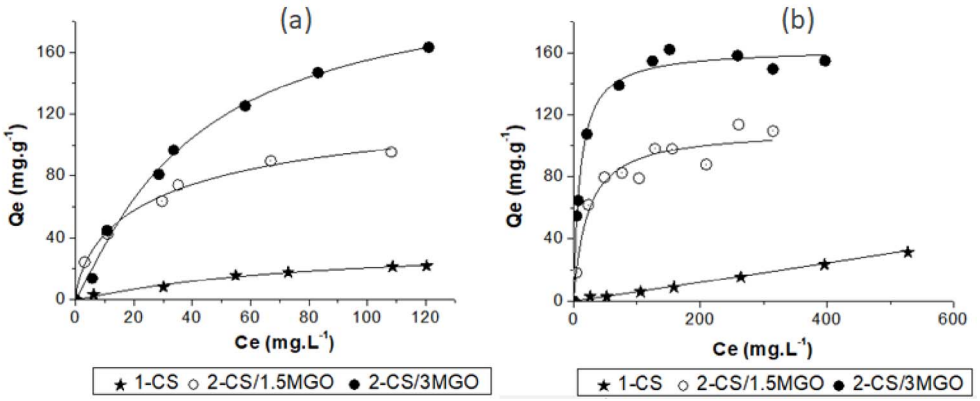

Figure 8. Adsorption isotherms of Zn^{2+} (a) and MTP (b) on pure and hybrid CS beads. The continuous lines represent calculated data using the best-fitting model.

Table 6. Adsorption isotherm parameters deducted from Langmuir, Freundlich and Langmuir–Freundlich model fitting

Model	Constants	Zn^{2+}			MTP		
		1-CS	2-CS/1.5MGO	2-CS/3MGO	1-CS	2-CS/1.5MGO	2-CS/3MGO
Langmuir	Q_{max} (mmol·g^{-1})	0.62 ± 0.08	1.67 ± 0.09	3.6 ± 0.2	0.2 ± 0.0	0.41 ± 0.02	0.608 ± 0.001
	K_L (L·mmol^{-1})	0.7 ± 0.2	3.9 ± 0.7	1.2 ± 0.2	0.49 ± 0.05	12 ± 3	25 ± 2
	R^2	0.989	0.985	0.994	0.94	0.954	0.991
	R_L	0.46	0.12	0.28	1	0.07	0.03
Freundlich	K_F (mmol$^{-1/n}$·L$^{1/n}$)	0.24 ± 0.01	1.29 ± 0.04	1.91 ± 0.07	0.059 ± 0.001	0.41 ± 0.02	0.60 ± 0.03
	n	1.6 ± 0.2	2.8 ± 0.3	1.8 ± 0.2	0.97 ± 0.03	3.7 ± 0.6	5.2 ± 0.9
	$1/n$	0.63	0.36	0.56	1.03	0.27	0.2
	R^2	0.980	0.981	0.969	0.997	0.929	0.92
Langmuir–Freundlich	Q_{max} (mmol·g^{-1})	0.5 ± 0.21	2.2 ± 0.4	3.2 ± 0.3	0.2	0.45 ± 0.07	0.61 ± 0.02
	K_{LF} (L·mmol^{-1})	0.9 ± 0.5	1.9 ± 1.1	1.7 ± 0.3	0.60 ± 0.02	10 ± 5	26 ± 3
	b	1.1 ± 0.3	0.7 ± 0.1	1.2 ± 0.1	1.5 ± 0.1	0.8 ± 0.2	1 ± 0.1
	R^2	0.987	0.993	0.994	0.996	0.952	0.990

complexation with the nitrogen amine group's free doublet. Zn^{2+} adsorption on CS/MGO hybrid beads can occur simultaneously by a multilayer mechanism both on CS and on MGO adsorption sites. In the hybrid beads, electrostatic interactions are indeed coupled with complexation, offering a large diversity and heterogeneity of adsorption sites.

If all the NH_2 sites of pure CS were occupied by Zn^{2+}, the adsorption capacity would reach a maximum value of 160 mg·g^{-1}. The adsorption isotherm and the adsorption uptake reached (40 mg·g^{-1}) confirm that only few available adsorption sites are really occupied on the CS chains and involved in the Zn^{2+} chelating. One explanation may come from the interactions between the CS chains which considerably reduce the number of free adsorption sites on the polymer chains. The counting of all the nitrogen doublets indicates that only 25% of the adsorption sites are really active. Nevertheless, CS chains can either be linked by complexation bond with amine groups of various chains or contain also hydroxyl groups which may be involved in Zn^{2+} adsorption mechanisms. Additionally, a Zn^{2+} cation can be chelated by several amine groups. These results suggest that for Zn^{2+} adsorption on CS at pH 6.5, the interactions through complexation prevail over the repulsive electrostatic interactions between the positively charged CS chains (around half of the NH_2

groups are either neutral or positively charged) and the metallic cations.

MGO material was selected because of its affinity towards divalent metallic cations. Indeed, maximum adsorption capacities in the range of 98–246 $mg{\cdot}g^{-1}$, and 30–346 $mg{\cdot}g^{-1}$ were reported for Pb^{2+} [6,14], and Zn^{2+} [6,43,44], respectively. Especially, the higher the amount of carboxylic groups in MGO, the higher the adsorption uptake of Zn^{2+} should be.

The Zn^{2+} adsorption isotherm of pure MGO was studied at pH = 4 to avoid the Zn hydroxide precipitation. Indeed, such precipitation was observed at pH 6.5 in the concentration range of 0–30 $mg{\cdot}L^{-1}$, as already reported by Sitko *et al.* [44] at pH = 7 in the concentration range of 100–300 $mg{\cdot}L^{-1}$. At pH = 4, an adsorption uptake of almost 30 $mg{\cdot}g^{-1}$ (0.38–0.46 $mmol{\cdot}g^{-1}$) was measured at concentrations in the range of 0 $mg{\cdot}L^{-1}$ to 300 $mg{\cdot}L^{-1}$. This value is comparable with the amount of carboxylate groups measured on our prepared MGO sample (0.44 $mmol{\cdot}g^{-1}$) which confirms they are the main groups involved in the adsorption mechanism. Our MGO adsorption capacity is far from the one of 346 $mg{\cdot}g^{-1}$ found by Sitko *et al.* [44]. This suggests that each MGO synthesis condition leads to a MGO having its singular properties, including peculiar oxygenated group types and amounts and therefore its own adsorption ability. Indeed, MGO prepared in this work possesses 1.4 $mmol{\cdot}g^{-1}$ dissociated carboxylic groups (at pH = 7). If all these sites were involved in Zn^{2+} adsorption, one would obtain a 92 $mg{\cdot}g^{-1}$ adsorption capacity.

According to the MGO amounts in the 2-CS/1.5MGO and 2-CS/3MGO hybrid beads (30 wt% and 46 wt%, respectively, thus approximately 1/3 and 1/2) and to the number of carboxylate sites on MGO (1.4 $mmol{\cdot}g^{-1}$), the adsorption capacity of these two kinds of beads should reach 56 $mg{\cdot}g^{-1}$ and 64 $mg{\cdot}g^{-1}$, respectively. This result shows that the higher the MGO amount in the hybrid beads, the higher the adsorption capacity. Moreover, one may notice a synergic effect between the CS matrix and the MGO charge, as far as MGO is dispersed between the CS chains and reduces the hydrogen bonding between the CS chains, CS adsorption sites may become therefore more available for Zn^{2+} adsorption. Indeed, CS also presents high metallic divalent cation adsorption capacities such as 10 $mg{\cdot}g^{-1}$ for Zn^{2+} [62] or 73 $mg{\cdot}g^{-1}$ for Pb^{2+} [63].

For the 2-CS/1.5MGO hybrid beads, the adsorption capacity is about 109 $mg{\cdot}g^{-1}$, practically twice the calculated value of 56 $mg{\cdot}g^{-1}$. This result means that MGO firstly acts as an adsorbent trapping Zn^{2+} and secondly as an active additive allowing a better accessibility for adsorption on the CS matrix sites.

For the 2-CS/3MGO hybrid beads, the 235 $mg{\cdot}g^{-1}$ measured adsorption capacity (Langmuir model) is also much higher than the 64 $mg{\cdot}g^{-1}$ theoretical value, calculated by considering all the MGO and CS potential adsorption sites. This demonstrates the synergic adsorption effect brought by MGO to the hybrid beads as far as each adsorbent is active and MGO is enhancing the CS adsorption efficiency. In the 2-CS/3MGO, all the MGO sites appear to be active for the cation adsorption.

3.3.3. *Interpretation of Metoprolol adsorption isotherms*

The MTP adsorption isotherm on pure CS beads (sample 1-CS) is better fitted by the Freundlich model (Table 6). The $n = 1$ value suggests that adsorption is not stimulated. Indeed, MTP adsorption on CS may occur through very weak interactions. This result is explained by the CS cationic NH_3^+ groups promoting rather repulsive interactions with the positively charged MTP. Besides, MTP cannot be adsorbed by complexation on $-NH_2$ sites of CS.

The MTP adsorption isotherm on raw MGO powder is fitted by Langmuir–Freundlich model (R^2 = 0.987). The $n = 3.5$ Freundlich coefficient value confirms a spontaneous adsorption through strong interactions. The adsorption capacity calculated from the MTP adsorption isotherm reaches 435 $mg{\cdot}g^{-1}$ (1.6 $mmol{\cdot}g^{-1}$). This high MTP adsorbed amount is related to the high number of MGO anionic sites (carboxylate groups = 1.4 $mmol{\cdot}g^{-1}$). If MTP had adsorbed only through electrostatic interactions, the maximum adsorption capacity value would have reached 374 $mg{\cdot}g^{-1}$. This result also suggests that MTP adsorption on MGO is achieved additionally by chelation through acceptor–donor interactions as with MGO Lewis bases. MTP adsorption on MGO takes places either by electrostatic or by acceptor–donor interactions but these two types of interactions cannot be quantified.

MTP adsorption isotherms on 2-CS/1.5MGO and 2-CS/3MGO hybrid beads are better simulated by

the Langmuir model (Table 6) implying the adsorbed MTP monolayer formation. Adsorption occurs on a relatively homogenous surface, involving mainly the anionic groups, which are among the main active groups on the MGO surface. The R_L values are between 0 and 1 indicating that MTP adsorption is spontaneous on the hybrid adsorbents. The high measured adsorption capacities (110 and 163 mg·g^{-1} for 2-CS/1.5MGO and 2-CS/3MGO respectively, Table 6) demonstrate that such hybrid materials are appropriate for MTP-like cationic organic molecule removal.

The 2-CS/1.5MGO and 2-CS/3MGO hybrid beads have an adsorption capacity of 110 mg·g^{-1} and 163 mg·g^{-1}, respectively. These values are close to the ones of 125 mg·g^{-1} and 188 mg·g^{-1} calculated by taking into account restrictively the proportion of carboxylate sites in 2-CS/1.5MGO and 2-CS/3MGO, respectively. This confirms that only MGO is an active material toward MTP adsorption on the hybrid beads, as previously found in kinetics studies.

According to the MGO proportion (MTP adsorption capacity of 435 mg·g^{-1}) in the hybrid beads, the 2-CS/1.5MGO and 2-CS/3MGO adsorption capacities should attain 145 mg·g^{-1} and 217 mg·g^{-1}, respectively, if all the MGO adsorption sites were fully accessible in the beads. This means that nearly 76% and 80% of the MGO adsorption sites remain active in the 2-CS/1.5MGO and 2-CS/3MGO composite materials, respectively. As mentioned previously, Cryo-SEM characterization showed that the MGO dispersion in the 2-CS/3MGO was not fully achieved, explaining a loss of accessibility of the MGO sites.

3.3.4. *Comparison of Zn^{2+} and MTP adsorption with the literature*

Tables 7 and 8 present the Zn^{2+} and MTP adsorption capacities of different materials from the literature, which are compared to our hybrid beads (sample 2-CS/3MGO).

As previously reported (Section 3.3.2), the zinc cation adsorption capacity on MGO depends on its synthesis method. The MGO prepared by Wang *et al.* [6] exhibits a 246 mg·g^{-1} Zn^{2+} adsorption capacity. The non-binding doublets of CS enable the removal of divalent cations in water, and Chen *et al.* [62] reported a 10 mg·g^{-1} maximum Zn^{2+} adsorption uptake. The hybrid adsorbents synthesized in this work exhibit Zn^{2+} adsorption capacities higher than most of previously reported ones. As an example, raw or modified bentonites show around 68 mg·g^{-1} adsorption uptake [64]. Most of the carbon materials (especially AC powders) show weak removal efficiencies for metallic cations. Indeed, carbon materials must be oxidized to develop cation exchange properties, such as ACs of wood origin oxidized by ammonium peroxodisulphate showing an adsorption capacity of 22.5 mg·g^{-1} [65]. In such functionalized carbon materials, porosity is not responsible for the adsorption but rather the anionic grafted acidic functions. An imprinted polymer supported on graphene oxide/CS magnetic nanocomposite (IIP-MGO/Chm) showed a 71.4 mg·g^{-1} zinc cation adsorption capacity [66].

For MTP abatement, the photocatalytic decomposition shows a high efficiency but is still a high-cost and largely controversial process [59]. Other materials, such as silica gels or nanoparticles (iron particles deposited on sepiolite) have been studied but they are still quite toxic, difficult to produce and show relatively low efficiencies (5 mg·g^{-1}) [67]. Clay minerals present low MTP adsorption capacities such as 7 mg·g^{-1} for kaolinite and 4 mg·g^{-1} for talc [17]. Hydrophobic AC exhibits a 320 mg·g^{-1} high adsorption efficiency [23]. Naghipour *et al.* [68] studied the MTP removal from water by an AC prepared from pine cones. The maximum adsorption capacity of this AC is 179 mg·g^{-1} [68] and in the same range as the 2-CS/3MGO adsorption capacity reported in this work.

3.4. *Beads' regeneration*

CS and MGO show a reversible adsorption. The cation desorption from CS may be achieved through the partial or total protonation of the amine groups, thereby reducing the number of electron doublets on nitrogen atoms of the polymer chains responsible for cations complexation. Similarly, the desorption of cations from MGO through electrostatic interactions on COO^- functions could be achieved by the carboxylate groups protonation in order to restore the carboxylic groups at acidic pH values.

In order to perform the CS/MGO beads regeneration without altering the mechanical properties (resistance of the beads to acidic environment limited by the CS dissolution below pH 4), a regeneration process at pH 4 was studied.

Table 7. Comparison of adsorption uptake of Zn^{2+} on 2-CS/3MGO and various materials

Adsorbent	Q_{ads} (mg·g^{-1})	Reference
MGO	246	[6]
Chitosan	10	[62]
Bentonite	68	[64]
Activated carbon oxidized by $(NH_4)_2S_2O_8$	22.5	[65]
IIP-MGO/Chm	71.4	[66]
2-CS/3 MMGO	235	This work

Table 8. Comparison of adsorption uptake of MTP on 2-CS/3MGO and various materials

Adsorbent	Q_{ads} (mg·g^{-1})	Reference
Talc	4	[17]
Kaolinite	7	[17]
Hydrophobic activated carbons	320	[23]
Iron particles supported on sepiolite	5	[67]
Activated carbon from pine cones	179	[68]
2-CS/3MGO	163	This work

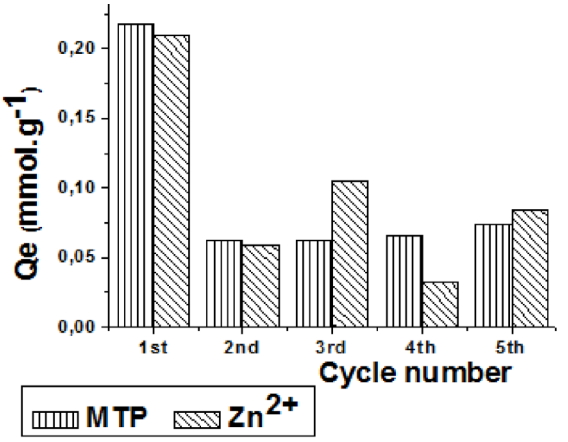

Figure 9. Adsorption capacity of 2-CS/1.5 MGO beads towards Zn^{2+} and MTP after a few cycles of regeneration.

After five cycles of adsorption/regeneration, the mechanical stability of the hybrid beads was still good. As shown in Figure 9, 35–40% of the initial adsorption capacity toward MTP or Zn^{2+} remains even after a few cycles. This difference may be explained by considering a few irreversible donor–acceptor interactions between MTP and MGO. The formation of hydrogen bonds between CS chains due to the protonation of NH_2 groups during the first cycle at pH 4 may lead to a modification of the arrangement of chains in the polymer and thus to a decrease in the number of active sites for Zn^{2+} which implies a loss of the quantity of the regenerable sites.

4. Conclusion

In this work hybrid materials based on CS and MGO in the form of hydrogel beads were successfully prepared to combine the numerous anionic MGO adsorption sites with the chelating properties offered by the CS amino groups. The CS matrix role in the dispersion of MGO particles is preserved even at high MGO content (CS/MGO ratio higher than 50/50 wt% for 2-CS/1.5MGO). The 2-CS/1.5MGO hybrid beads show good mechanical properties and a homogenous MGO dispersion within the CS polymer matrix, as evidenced by the results of Cryo-SEM analyses. Moreover, as shown by nitrogen gas adsorption measurement, MGO addition significantly increases the porosity of the 2-CS/1.5MGO beads in comparison to pure CS.

Zn^{2+} and MTP adsorption kinetics can be fitted both by the pseudo-first- and second-order models. The MGO/CS blending leads to a decrease in the adsorption speed explained by the kinetics limitation due to the diffusion toward the MGO sites depending

on their accessibility and related to the porosity of the materials.

The MTP adsorption isotherm on the pure CS beads (1-CS) is better simulated by the Freundlich model indicating that CS is not efficient for the MTP adsorption.

The Langmuir model better fits the MTP adsorption isotherms on the hybrid 2-CS/1.5MGO and 2-CS/3MGO adsorbents (R^2 values between 0.94 and 0.99), showing maximum adsorption uptakes of 110 and 163 mg·g^{-1} respectively. The MTP adsorption kinetics and isotherms are in good agreement with the MTP trapping on the MGO anionic sites (carboxylate groups) occurring through electrostatic interactions.

The 2-CS/1.5MGO and 2-CS/3MGO hybrid beads are very efficient for MTP and Zn^{2+} abatements as well. The Zn^{2+} adsorbed amounts are much higher for 2-CS/3MGO (236 mg·g^{-1}) than for the pure CS beads (40 mg·g^{-1} calculated using the Langmuir model), thus demonstrating the synergic effects brought by MGO incorporation in the hybrid beads. In these beads, two kinds of Zn^{2+} adsorption sites are identified: MGO carboxylate groups giving electrostatic interactions, and CS amine groups yielding Zn^{2+} complexation. The Zn^{2+} adsorption signature on these two types of sites is both the Langmuir–Freundlich shape of the isotherm and the decrease in Zn^{2+} adsorption kinetics on increasing its concentration, owing to the adsorption shift from MGO sites to CS ones. A way to improve the Zn^{2+} adsorption could be to identify better the chemical groups involved in the adsorption mechanism and then to increase their amount in MGO by tailoring its synthesis.

The adsorption of the MTP-Zn^{2+} mixture does not affect the adsorption efficiency of the hybrid CS beads. For 0.75 mmol·L^{-1} and 1.5 mmol·L^{-1} initial concentrations, the adsorption of each species still occurs without any competition. Competition effects are observed at 2 mmol·L^{-1}, as hybrid beads are more efficient for Zn^{2+} adsorption than for MTP adsorption.

The prepared hybrid CS/MGO beads show high adsorption efficiencies towards Zn^{2+} and MTP with relatively high measured maximum adsorption values, as compared to other adsorbents. As far as the beads could be used in fixed bed reactors, they could more easily be applied in a treatment plant process than a MGO powder. These materials are therefore good candidates as adsorbents for water treatment purposes. The CS/MGO hybrid adsorbents show higher efficiency for Zn^{2+} abatement than for MTP, in agreement with the higher Zn^{2+} concentrations encountered in natural water samples.

Additionally, the prepared hybrid adsorbents can be regenerated easily, and their adsorption properties are relatively well preserved after five adsorption/regeneration cycles (35–40%) without altering their mechanical properties. The regeneration level is limited by the CS stability pH domain. In future works the regeneration ability may be increased by the reticulation of CS polymer chains though it may affect the adsorption uptakes.

This work concludes that CS/MGO composite adsorbents are appropriate for the treatment of metallic (like Zn^{2+}) and organic (like MTP) cations in water. The efficiency is higher for Zn^{2+} abatement than for MTP owing to some pronounced synergic effects between CS and MGO. In contrast to the high-cost photo-catalytic methods that generate noxious by-products, the biodegradable and non-toxic hybrid materials proposed in this work are easy to produce, using a low-cost process and exhibit high renewability.

Conflicts of interest

Authors have no conflict of interest to declare.

Acknowledgements

We gratefully acknowledge the financial support provided to the PIVOTS project and to the APR-IR MatHéO project by the "Région Centre – Val de Loire".

References

[1] S. Tunali, T. Akar, *J. Hazard. Mater. B*, 2006, **131**, 137-145.
[2] T. Deblonde, C. Cossu-Leguille, P. Hartemann, *Int. J. Hyg. Environ. Health*, 2011, **214**, 442-448.
[3] D. Bendz, N. A. Paxeus, T. R. Ginn, F. J. Loge, *J. Hazard. Mater.*, 2005, **122**, 195-204.
[4] V. Romero, P. Marco, J. Giménez, S. Esplugas, *Int. J. Photoenergy*, 2013, **10**, 1-11.
[5] V. Sarin, K. K. Pant, *Bioresour. Technol.*, 2006, **97**, 15-20.
[6] H. Wang, X. Yuan, Y. Wuc, H. Huang, G. Zeng, Y. Liu, X. Wang, N. Lin, Y. Qi, *Appl. Surf. Sci.*, 2013, **279**, 432-440.
[7] M. Soylak, S. Saracoglu, U. Divrikli, L. Elci, *Talanta*, 2005, **66**, 1098-1102.
[8] M. Soylak, M. Tuzen, *J. Hazard. Mater.*, 2008, **152**, 656-661.
[9] M. Hunsom, K. Pruksathorn, S. Damronglerd, H. Vergnes, P. Duverneuil, *Water Res.*, 2005, **39**, 610-616.

[10] Y. Chen, B. Pan, H. Li, W. Zhang, L. Lv, J. Wu, *Environ. Sci. Technol.*, 2010, **44**, 3508-3513.

[11] V. Romero, O. Mgonzález, B. Bayarri, P. Marco, J. Giménez, S. Esplugas, *Catal. Today*, 2015, **240**, 86-92.

[12] Y. Yu, Y. Liu, X. Wu, Z. Weng, Y. Hou, L. Wu, *Sep. Purif. Technol.*, 2015, **142**, 1-7.

[13] S. Hydari, H. Sharififard, M. Nabavinia, M. R. Parvizi, *Chem. Eng. J.*, 2012, **193-194**, 276-282.

[14] L. Liu, C. Li, C. Bao, Q. Jia, P. Xiao, X. Liu, Q. Zhang, *Talanta*, 2012, **93**, 350-357.

[15] H. A. Shawky, A. H. M. El-Aassar, D. E. Abo-Zeid, *J. Appl. Polym. Sci.*, 2012, **125**, 93-101.

[16] S. F. Soares, T. R. Simões, M. António, T. Trindade, A. L. Daniel-da Silva, *Chem. Eng. J.*, 2016, **302**, 560-569.

[17] Z. Li, N. M. Fitzgerald, Z. Albert, A. Schnabl, W. T. Jiang, *Chem. Eng. J.*, 2015, **272**, 48-57.

[18] M. Ghayaza, L. Le Forestier, F. Muller, C. Tournassat, J. M. Beny, *J. Colloid Interface Sci.*, 2011, **361**, 238-246.

[19] L. Monser, N. Adhoum, *Sep. Purif. Technol.*, 2002, **26**, 137-146.

[20] X. Guo, S. Zhang, X. Shan, *J. Hazard. Mater.*, 2008, **151**, 134-142.

[21] Y. Wu, S. Zhang, X. Guo, H. Huang, *Bioresour. Technol.*, 2008, **99**, 7709-7715.

[22] X. Chen, K. F. Lam, S. F. Mak, K. L. Yeung, *J. Hazard. Mater.*, 2011, **186**, 902-910.

[23] F. Bouyahmed, M. Cai, L. Reinert, L. Duclaux, R. K. Dey, H. Benyoucef, M. Lahcini, F. Muller, S. Delpeux-Ouldriane, *J. Carbon Res.*, 2018, **4**, 35-46.

[24] G. Crini, P. M. Badot, E. Grubal, *Chitin et chitosanchitosanchitosan du biopolymère à l'application*, Presses Universitaires de Franche-Comté, Besançon, France, 2009, 10-30 pages.

[25] G. N. Kousalya, M. R. Gandhi, S. Meenakshi, *Int. J. Biol. Macromol.*, 2010, **47**, 308-315.

[26] M. R. Lasheen, I. Y. El Sherif, M. E. Tawfik, S. T. El-Wakeel, M. F. El-Shahat, *Mater. Res. Bull.*, 2016, **80**, 344-350.

[27] T. Phaechamud, J. Charoenteeraboon, *Am. Assoc. Pharm. Sci.*, 2008, **9**, 149-162.

[28] G. Rojas, J. Silva, J. A. Flores, A. Rodriguez, M. Ly, H. Maldonado, *Sep. Purif. Technol.*, 2005, **44**, 31-36.

[29] G. Karthikeyan, K. Anbalagan, N. M. Andal, *J. Chem. Sci.*, 2004, **116**, 119-127.

[30] P. Ding, K. L. Huang, G. Y. Li, Y. F. Liu, W. W. Zeng, *Int. J. Biol. Macromol.*, 2006, **39**, 222-227.

[31] F. N. Allouche, E. Guibal, N. Mameri, *Colloids Surf. A: Physicochem. Eng. Asp.*, 2014, **446**, 224-232.

[32] V. K. Mourya, N. N. Inamdar, *React. Funct. Polym.*, 2008, **68**, 1013-1051.

[33] G. Crini, P. M. Badot, *Prog. Polym. Sci.*, 2008, **33**, 399-447.

[34] M. J. Ahmed, B. H. Hameed, E. H. Hummadi, *Carbohydr. Polym.*, 2020, **247**, article no. 116690.

[35] W. Jiang, W. Wang, B. Pan, Q. Zhang, W. Zhang, L. Lv, *ACS Appl. Mater. Interfaces*, 2014, **6**, 3421-3426.

[36] W. M. Almgothmi, N. M. Bandaru, Y. Yu, J. G. Shapter, A. V. Ellis, *J. Colloid Interface Sci.*, 2013, **397**, 32-38.

[37] N. A. Travlou, G. Z. Kyzas, N. K. Lazaridis, E. A. Deliyanni, *Chem. Eng. J.*, 2013, **217**, 256-265.

[38] X. Ren, J. Li, X. Tan, X. Wang, *Dalton Trans.*, 2013, **42**, 5266-5274.

[39] S. T. Yang, S. Chen, Y. Chang, A. Cao, Y. Liu, H. Wang, *J. Colloid. Interface Sci.*, 2011, **359**, 24-29.

[40] N. Zhang, H. Qiu, Y. Si, W. Wang, J. Gao, *Carbon*, 2011, **49**, 827-837.

[41] H. Yan, X. Tao, Z. Yang, K. Li, H. Yang, A. Li, R. Cheng, *J. Hazard. Mater.*, 2014, **268**, 191-198.

[42] D. Robati, B. Mirza, M. Rajabi, O. Moradi, I. Tyagi, S. Agarwal, V. K. Gupta, *Chem. Eng. J.*, 2016, **284**, 687-697.

[43] N. H. Othman, N. H. Alias, M. Z. Shahruddin, N. F. Abu Bakar, N. R. N. Him, W. J. Lau, *J. Environ. Chem. Eng.*, 2018, **6**, 2803-2811.

[44] R. Sitko, E. Turek, B. Zawisza, E. Malicka, E. Talik, J. Heimann, A. Gamgor, B. Feist, R. Wrzalik, *Dalton Trans.*, 2013, **42**, 5682-5689.

[45] Y. C. Lee, J. W. Yang, *J. Ind. Eng. Chem.*, 2012, **18**, 1178-1185.

[46] H. N. Catherin, M. H. Ou, B. Manu, Y. Shih, *Sci. Total Environ.*, 2018, **635**, 629-638.

[47] M. S. Samuel, S. S. Shah, J. Bhattacharya, K. Subramaniam, N. D. P. Singh, *Int. J. Biol. Macromol.*, 2018, **115**, 1142-1150.

[48] Y. Chen, H. Bai, L. Li, *J. Mater. Chem. A*, 2013, **1**, 1992-2001.

[49] Y. Jiang, J. L. Gong, G. M. Zeng, X. M. Ou, Y. N. Chang, C. H. Deng, J. Zhang, H. Y. Liu, S. Y. Huang, *Int. J. Biol. Macromol.*, 2016, **82**, 702-710.

[50] M. A. Kamal, S. Bibi, S. W. Bokhari, A. H. Siddique, T. Yasin, *React. Funct. Polym.*, 2017, **110**, 21-29.

[51] H. H. Najafabadi, M. Irani, L. R. Rad, A. Heydari, H. I. Haririan, *R. Soc. Chem.*, 2015, **5**, 16532-16539.

[52] W. Zhang, C. Zhou, W. Zhou, A. Lei, Q. Zhang, Q. Wan, B. Zou, *Bull. Environ. Contam. Toxicol.*, 2011, **87**, 86-90.

[53] L. Fan, C. Luo, M. Sun, X. Li, H. Qiu, *Colloids Surf. B: Biointerfaces*, 2013, **103**, 523-529.

[54] G. Z. Kyzas, N. A. Travlou, E. A. Deliyanni, *Colloids Surf. B: Biointerfaces*, 2014, **113**, 467-476.

[55] W. Gao, M. Majumder, L. B. Alemany, T. N. Narayanan, M. A. Ibarra, B. K. Pradhan, P. M. Ajayan, *ACS Appl. Mater. Interfaces*, 2011, **3**, 1821-1826.

[56] E. Kazemi, S. Dadfarnia, A. M. H. Shabani, M. Ranjbar, *Food Chem.*, 2017, **237**, 921-928.

[57] C. N. Nupearachchi, K. Mahatantila, M. Vithanage, *Groundw. Sustain. Dev.*, 2017, **5**, 206-215.

[58] W. S. Hummers, R. E. Offeman, *J. Am. Chem. Soc.*, 1958, **80**, 1339.

[59] S. Kutzner, M. Schaffer, H. Bornick, T. Licha, E. Worch, *Water Res.*, 2014, **54**, 273-283.

[60] H. Ge, Z. Ma, *Carbohydr. Polym.*, 2015, **131**, 280-287.

[61] J. Zhang, Y. Yu, D. Huang, *Solid State Sci.*, 2010, **12**, 1183-1187.

[62] A. H. Chen, S. C. Liu, C. Y. Chen, C. Y. Chen, *J. Hazard. Mater.*, 2008, **154**, 184-191.

[63] G. Gyananath, D. K. Balhal, *Cellul. Chem. Technol.*, 2012, **46**, 121-124.

[64] T. K. Sen, D. Mgomez, *Desalination*, 2011, **267**, 286-294.

[65] Y. Dai, K. Zhang, J. Li, Y. Jiang, Y. Chen, S. Tanaka, *Sep. Purif. Technol.*, 2017, **186**, 255-263.

[66] E. Kazemi, S. Dadfarnia, A. M. H. Shabani, M. Ranjbar, *Food Chem.*, 2017, **237**, 921-928.

[67] M. Daneshkhah, H. Hossaini, M. Malakootian, *J. Environ. Chem. Eng.*, 2017, **5**, 3490-3499.

[68] D. Naghipour, A. Amouei, K. T. Ghasemi, K. Taghavi, *Environ. Health Eng. Manag. J.*, 2019, **6**, 81-88.